Modification in adsorption properties of graphene during the development of viral biosensors

© I.A. Eliseev[1], E.A. Gushchina[1], S.A. Klotchenko[2], A.A. Lebedev[1], N.M. Lebedeva[1], S.P. Lebedev[1], A.V. Nashchekin[1], V.N. Petrov[1], M.V. Puzyk[3], A.D. Roenkov[4], A.N. Smirnov[1], E.M. Tanklevskaya[1], A.S. Usikov[4,5], E.I. Shabunina[1], N.M. Schmidt[1,¶]

[1] Ioffe Institute,
194021 St. Petersburg, Russia
[2] Smorodintsev Research Institute of Influenza, Ministry of Health of the Russian Federation,
197376 St. Petersburg, Russia
[3] Herzen State Pedagogical University of Russia,
191186 St. Petersburg, Russia
[4] Nitride Crystals Group,
194156 St. Petersburg, Russia
[5] ITMO University,
197101 St. Petersburg, Russia
¶ E-mail: natalia.shmidt@mail.ioffe.ru

Received December 9, 2022
Revised December 15, 2022
Accepted December 28, 2022

The well-known effect of the local interaction between graphene and photoresist (LIGF) during the creation of biosensors is shown to lead to non-uniform distribution of compressive stresses, which deteriorates the adsorption properties of graphene, parameter reproducibility, and detecting ability of influenza B and SARS-Cov-2 biosensors. It is also shown that controlling the occurrence of LIGF areas on a graphene surface by atomic force microscopy or introducing a protective layer between graphene and photoresist can minimize the non-persistent effect of LIGF. The results of influenza B and SARS-CoV-2 imaging on the graphene surface in biosensor chips in a scanning electron microscope are presented.

Keywords: graphene, biosensors, SARS-CoV-2, influenza virus B.

DOI: 10.21883/SC.2022.12.55150.4429

1. Introduction

Unique properties of graphene make this low-dimensional material suitable for the design of biosensors for influenza and SARS-CoV-2 viruses [1–3]. Studies into the enhancement of reproducibility of biosensor parameters [3,4] are performed alongside with the examination of characteristics of the initial graphene material and basic biosensor fabrication operations. The high sensitivity of adsorption properties of graphene to physical and chemical influences and strain fluctuations [5] may make the parameters of biosensors at the key stages of their production irreproducible. The initial stage involves the fabrication of chips of a specific geometry from a graphene film with two (resistor) or three (transistor) Ohmic contacts. Controlled processing (functionalization) of the graphene surface is carried out next to form covalent bonds that enable selective chemical reactions of biomolecule (antibody) binding [1–8].

The immobilization (binding) of the corresponding antibodies on functionalized graphene establishes the conditions for an antibody–antigen (virus) immune reaction on the graphene surface in a chip for detection of viruses in an aqueous solution of sodium chloride (anolyte). The antibody–antigen (virus) immune reaction on the surface of graphene alters its electron state, and this change may be detected, e.g., by measuring the current flowing through a chip based on a graphene film. Electrochemical methods may be used at this stage to detect viruses on the graphene surface.

The limit sensitivity of a biosensor of this kind is specified by the properties of graphene and physicochemical processes proceeding on the graphene surface within the entire production cycle; it also depends on the degree of uniformity of these processes over the graphene chip area. It should be noted that inactivated influenza B viruses were used in the examination of biosensors; the term „virus“ is used below for simplicity. Photolithography (PLG) is used at the initial stage of biosensor fabrication. The results of studies [9,10] performed throughout the world revealed that graphene interacts with the photoresist in the process of PLG, forming local regions with resist residue (LRRs), which is hard to remove from the graphene surface. The graphene surface roughness increases as a result. This problem cannot be solved completely by selecting a specific photoresist, since the interaction proceeds at the level of benzene rings that are present in all types of photoresists used and in graphene (regardless of the method of its production) [11]. The issue is exacerbated by the fact that the traditional optical microscopic technique used to verify the removal of a photoresist is insensitive to LRRs.

Atomic force microscopy (AFM) and Raman spectroscopy provide the most comprehensive data on LRRs [11]. One of the ways to solve the discussed problem consists in introducing a protective layer (PL) between graphene and the photoresist to limit their interaction [12,13]. Promising results were obtained in AFM and Raman studies of chips with a PL [12]. However, almost no data on the degree of preservation of the initial adsorption properties of graphene after PLG with a PL and on the enhancement of detection efficiency for influenza and SARS-CoV-2 viruses have been published. It should also be noted that most studies were performed for epitaxial graphene layers.

In the present paper, we report experimental data on the properties of graphene, which was synthesized by thermal decomposition on SiC substrates, before and after patterning of a biosensor chip. The influence of LRRs on the reproducibility of biosensor chip parameters and on the adsorption and detection characteristics of graphene in chips was revealed.

2. Experiment procedure

Studies were performed for chips with two contacts (graphene resistances) 1.5×2 mm in size mounted on a fabric-reinforced plastic holder. The sensing area (working area of graphene in a chip) was 1×1.5 mm. The biosensor chip design was detailed in [14]. Chips were fabricated from several wafers with graphene films formed by thermal decomposition of semi-insulating 4*H*-SiC substrates. Comprehensive data on the processing of chips and their mounting on holders were provided in [14].

2.1. Synthesis of graphene films on the surface of SiC by sublimation

Semi-insulating 4*H*-SiC substrates with a minimum misalignment angle ($\alpha \sim 0$) were used in our experiments; growth was performed in the (0001) orientation $\pm 0.25^\circ$ (Si face). Pre-growth etching in hydrogen atmosphere was carried out for preliminary cleaning of the SiC substrate surface. A gas mixture of argon (with a volume fraction of 95%) and hydrogen (5%) was used. Graphene was then grown on the SiC surface at a temperature of $1700-1800^\circ$C in argon atmosphere (720−750 Torr) in a black-lead crucible with induction heating.

2.2. Topographic patterning of biosensor chips on graphene/SiC wafers

Photolithography techniques and the AZ1318 photoresist were used for topographic patterning of chips on graphene/SiC wafers. The photoresist was removed in acetone. In addition to the traditional optical microscopic monitoring of photoresist removal, the surface of as-synthesized graphene on the wafer and graphene after PLG was examined by AFM. Experiments were also carried out with an LOR-10B PL introduced between the photoresist and graphene to prevent them from interacting with each other. The protective layer was removed in a diluted developing solution (1% alkali solution). Layers of Ti/Au (2/200 nm) were deposited to form Ohmic contacts [14].

2.3. Forming a biosensor chip based on the graphene/SiC structure

Graphene functionalization [7,8] is a common method for production of graphene chips with a sensory capacity. Covalent bonds forming on the graphene surface in the process of functionalization enable chemical reactions of specialized protective protein and (or) antibody binding. We have chosen covalent functionalization as a method that is the simplest and the most reliable and affordable. In the present study, the graphene surface was functionalized in two stages: covalent bonds were first formed in deposition of nitrophenyl groups (nitrobenzene, $C_6H_5NO_2$) and then reduced to phenylamine groups (aminobenzene, $C_6H_5NH_2$) by cyclic voltammetry. The process of graphene functionalization was detailed in [15].

Following surface functionalization, all chips were incubated in a solution containing monoclonal antibodies to the nucleoprotein of influenza B virus for 3 h at 37°C and rinsed once with phosphate-buffered saline (PBS). Influenza B and SARS-CoV-2 virus antigens in PBS were then detected. The concentration of influenza B virus in PBS was $10^{-14}-10^{-9}$ g/mL. It should be noted that the procedures of antibody binding and detection for influenza B and SARS-CoV-2 viruses differ only in the type of antibodies and antigens used. Antibodies to the NPs of influenza B and SARS-CoV-2 viruses were clones 6G1 and 3CV4, respectively.

Antibodies in the same concentration in a buffer solution were used in all experiments for immobilization of antibodies on the functionalized graphene surface. The concentration of monoclonal antibodies in PBS was 200 μg/mL. This concentration was higher than the one of possible sites with nitro groups suitable for antibody binding.

2.4. Detection of viruses

The Brisbane/46/15 strain of influenza B from the virus museum collection of the Smorodintsev Research Institute of Influenza of the Ministry of Health of the Russian Federation were used in detection tests. All experiments with viruses were performed in a BSL-2 setup at the Smorodintsev Research Institute of Influenza by its research staff members who co-authored the present paper.

Lysates (a mixture of antigens derived from inactivated viruses) of purified virus concentrates were used as an anolyte. These lysates were produced by dissolving viruses in a lysis buffer (200 mM DTT, 0.05% Tween 20 in PBS) with subsequent freezing and thawing. Since virus lysates of this kind mostly contain disrupted virions (fully formed virus particles consisting of a nucleic acid and a lipidic envelope (capsid) and residing outside of a living cell),

the concentration of viruses in them was estimated by measuring the total viral protein by the modified Lowry method with an RC DC Protein Assay Kit („Bio-Rad", United States). Anolyte solutions were prepared by decimal dilutions in PBS. The incubation with anolytes was performed at room temperature.

The biosensor operation in our experiments relies on an antigen–antibody immune reaction on the surface of graphene. Detection selectivity is largely attributable to the nature of an immune reaction: only affine (matching) antigens and antibodies are involved in the interaction and may alter the electric properties of graphene. However, other viruses may influence the biosensor response via different (not related to the immune reaction) mechanisms.

The response of biosensors with immobilized antibodies was examined in diluted solutions of the corresponding antigens in order to clarify the influence of the graphene surface on detection. A DC voltage of $20-80$ mV was applied in experiments to a graphene chip coated with antibodies to the nucleoproteins of influenza B or SARS-CoV-2 viruses. The chip was immersed into a diluted PBS solution of influenza B virus (containing the nucleoprotein antigen) for 30 s. The nucleoprotein of influenza B virus binds chemically to its complementary antibody, thus altering the graphene channel resistance, and this alteration may be detected rapidly by monitoring the current flow through the graphene/SiC chip.

2.5. Research methods

Current–voltage curves (CVCs) and Raman spectra, which provide data on the structural properties of graphene films, were examined for the initial chips based on graphene films and at each subsequent stage of biosensor fabrication. The surface morphology and the surface potential distribution were determined by AFM and Kelvin probe force microscopy (KPFM). Scanning electron microscopy (SEM) was also used to visualize the binding of antibodies and influenza viruses to the graphene surface.

AFM and KPFM measurements were performed in an Ntegra AURA microscope (NT-MDT, Russia). An HA_FM cantilever (www.tipsnano.com) was used in AFM studies, which were carried out in the resonance semicontact mode at a scan frequency and rate of 0.6 Hz and 1.3 μm/s, respectively. The force constant of this cantilever is 3.5 N/m, the curvature radius is ~ 10 nm, and the scan field size is 256×256 points.

CVCs were measured using a KEITHLEY 6487 power supply. SEM images of the chip surface were obtained in a JSM 7001F microscope (Jeol, Japan) in the secondary electron mode at an accelerating voltage of 5 kV and a beam current of 12 pA.

Raman spectra were measured at room temperature in the backscattering geometry with a Horiba LabRAM HREvo UV-VIS-NIR-Open spectrometer fitted with a confocal microscope. The power of a YAG:Nd laser with a wavelength of 532 nm was limited to 1.0 mW within a spot 1 μm in diameter in order to protect graphene films from damage and modification. Alongside with local measurements, sample regions $10 \times 10\,\mu$m in size were analyzed with subsequent plotting of Raman maps and histograms of parameters of spectral lines.

3. Experimental results

The graphene surface topography was monitored by AFM at all stages of fabrication of a graphene chip and its conversion into a viral infection sensor (i.e., after synthesis of a graphene film, metallization of contact regions, deposition and removal of the photoresist, and cutting the wafer into chips). The surface of assembled chips was also examined before and after detection of viral antigens. The root-mean-square roughness (rms) of the graphene surface within scan fields 10×10 and $2 \times 2\,\mu$m in size served as a quantitative characteristic of the morphology variation.

Figure 1, *a* shows the graphene surface topography in a chip after photolithography with AFM monitoring of the photoresist residue removal after all chip fabrication (processing) procedures, which involved $3-4$ resist deposition and removal operations. Non-uniformly distributed LRRs (bright regions of various shapes and sizes in the image) emerged following the photoresist removal, and the rms parameter increased relative to the initial values for a wafer with graphene before PLG. This rms increase reached an order of magnitude in certain 10×10 and $2 \times 2\,\mu$m scan fields.

The presence of LRRs on the graphene surface disrupts the reproducibility of resistance of chips fabricated from the same wafer. Figure 2 presents histograms of the resistance distribution for chips fabricated from two wafers. Blue columns represent the spread of resistance from 1.8 to 4 Ω for chips from the wafer with a non-uniform LRR distribution and the rms parameter varying from 1.4 (before PLG) to 12 nm (after PLG).

Two methods for abating the LRR contamination of the graphene surface were tested: (1) reduction of the number of PLG cycles with AFM monitoring of the photoresist removal after each PLG; (2) introduction of a PL between graphene and the photoresist in each photoresist deposition cycle. Both methods provided a reduction in the number of LRRs and leveled out the difference in rms values between graphene surfaces before and after PLG. A typical image of such a graphene surface in a chip is shown in Fig. 1, *b*. It was found that chips fabricated from wafers subjected to an optimized PLG procedure had significantly lower resistance values, and the spread of resistance of chips from the same wafer also decreased considerably (to $1-1.5\,\Omega$; see red columns in the histogram in Fig. 2).

Examining the Raman spectra of chips with different rms values (1.4 and 12 nm; see Fig. 3), we found that LRRs do not only reduce the graphene film area adsorbing antibodies and viral antigens, but also induce non-uniform

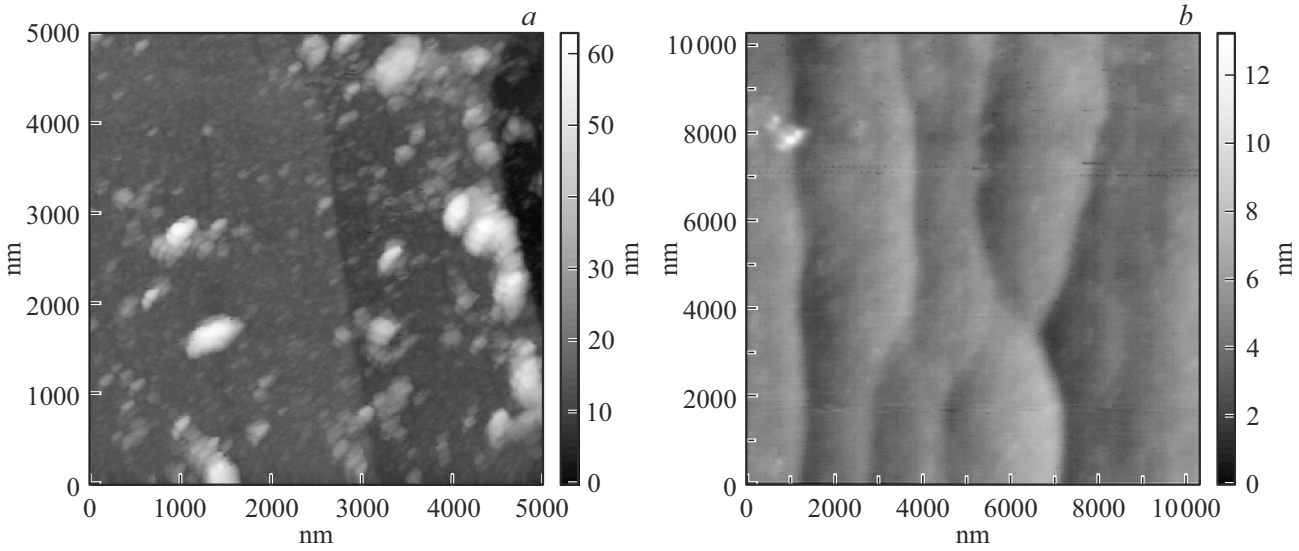

Figure 1. AFM images of the graphene surface topography in chips in a $10 \times 10\,\mu$m scan field: *a* — after multiple cycles of photoresist deposition and removal in chip processing, rms = 12 nm, and *b* — after optimization of the photolithography process, rms = 1.4 nm.

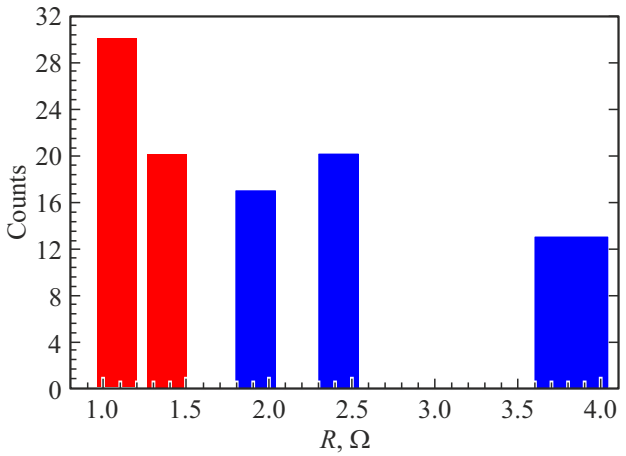

Figure 2. Histogram of the resistance distribution for biosensor chips on EG402 (blue columns) and EG417 (red columns) wafers. A total of 50 chips were fabricated from each wafer. (A color version of the figure is provided in the online version of the paper).

distributions of compressive stresses and carrier density in graphene films.

It should be noted that the spectra in Fig. 3 reveal high quality of graphene in chips, which is evidenced by the ratio of intensities of *G* and 2*D* lines and the lack of a *D* line that is associated with defects [16,17]. The distribution of FWHM values of the 2*D* line within an area of $10 \times 10\,\mu$m [18] demonstrates that monolayer graphene in chips contains no more than 30% of bilayer graphene. Well-known relations presented in [19] allow one to derive distribution maps of biaxial stresses ($\varepsilon_{\|}$) and free electron density (n_e) in graphene films in chips from Raman spectroscopy data.

Histograms of distribution of compressive stresses in chips with different rms values are shown in the insets in Fig. 3. Chips with rms = 12 nm and a large amount of LRRs feature a fairly wide spread of compressive stress values (from 0 to -0.25%), while the electron density varies within the range of $(1-8) \cdot 10^{12}\,\mathrm{cm}^{-2}$. The distributions for chips with rms = 1.4 nm, which is close to the initial values on a wafer, are significantly narrower: from -0.16 to -0.3% in compressive stress and from $4 \cdot 10^{12}$ to $8 \cdot 10^{12}\,\mathrm{cm}^{-2}$ in electron density.

The same chips differing greatly in the amount of LRRs and rms values were subjected simultaneously to all subsequent graphene surface processing procedures (functionalization and immobilization of antibodies to viral antigens) and to experiments on virus detection. The procedure of virus detection was detailed in Section 2.4. A set of dilutions of influenza B virus and the SARS-CoV-2 NP in PBS with concentrations of 10^{-9}, 10^{-10}, 10^{-11}, 10^{-12}, and 10^{-13} g/mL was used. The current flowing through the chip was measured for each virus concentration, and the concentration dependence of current (resistance) was plotted. It is commonly believed that a concentration dependence of the biosensor signal serves as evidence of binding of a viral antigen to an antibody immobilized on the graphene surface (even if the dependence is nonlinear in nature [20]). Chips with their rms values after PLG being several times higher than the initial ones do not normally reveal a concentration dependence of the biosensor signal. The best results in terms of virus detection were obtained in tests of chips with rms values after PLG differing by no more than 30% from the initial ones. These chips do not only manifest a concentration dependence, but also feature new (compared to the initial surface topology in Fig. 1, *b*) local regions of a predominantly spherical shape in AFM

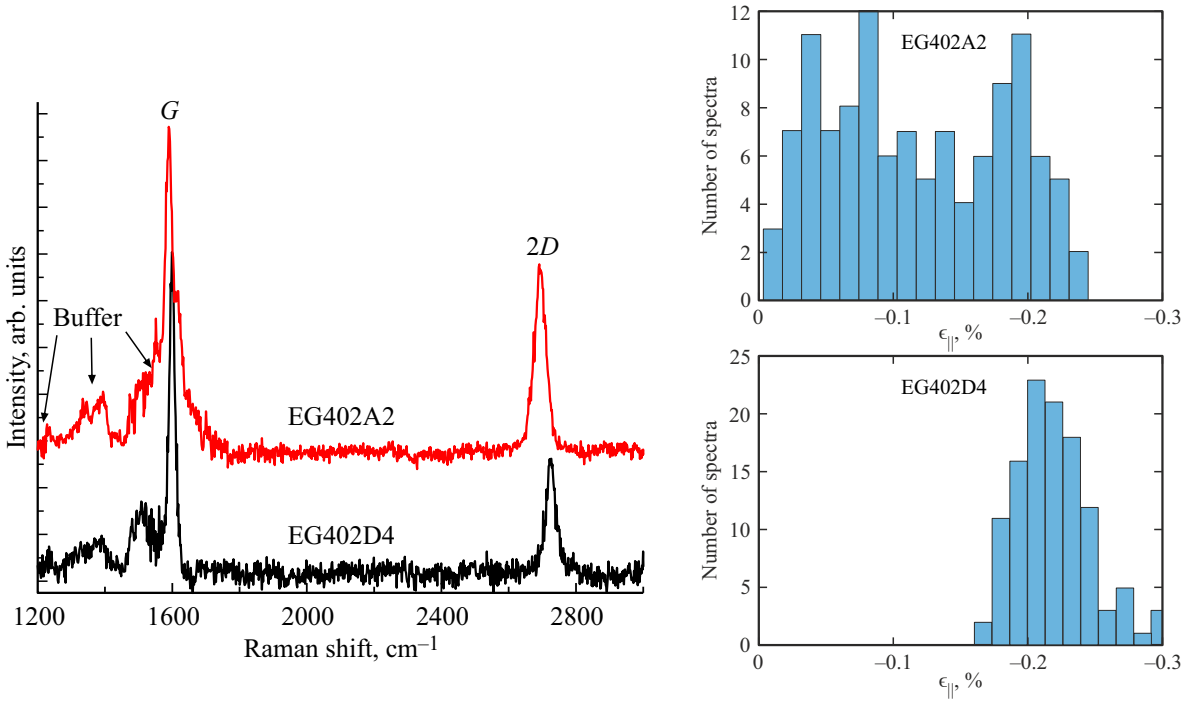

Figure 3. Typical Raman spectra of graphene in two chips with different rms values. The black curve corresponds to an EG402D4 chip with a small amount of LRRs (rms = 1.4 nm). The histogram of distribution of compressive stresses is shown in the inset. The red curve corresponds to an EG402A2 chip with a large amount of LRRs (rms = 12 nm). The histogram of distribution of compressive stresses is shown in the inset.

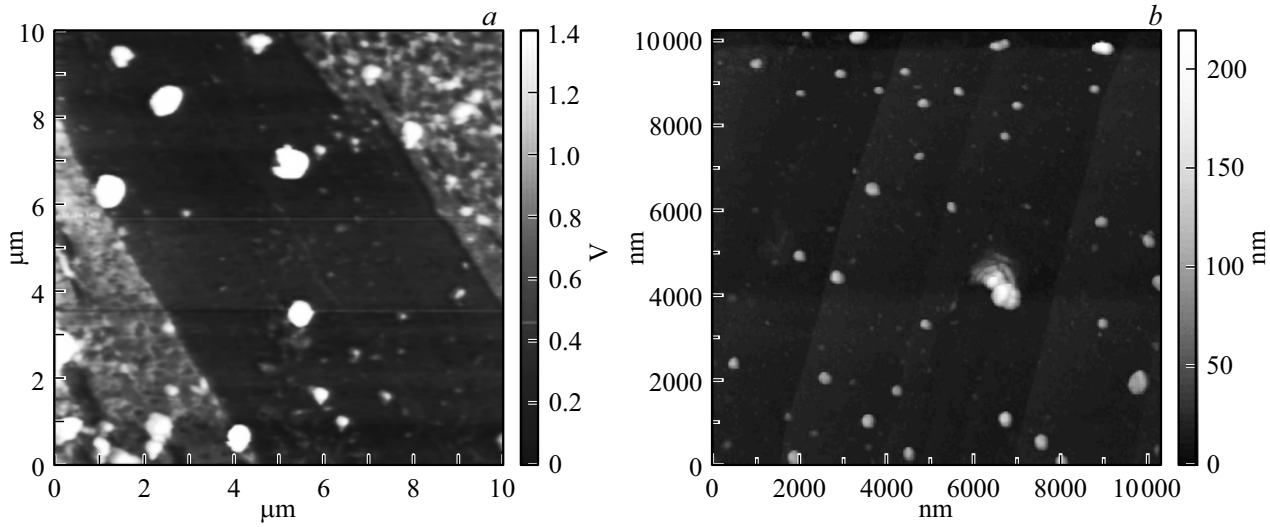

Figure 4. AFM images of the graphene surface in chips after detection of influenza B (*a*) and SARS-CoV-2 (*b*) viruses with similar concentrations of 10^{-9} g/mL.

images (Fig. 4) in 10×10 and $2 \times 2\,\mu$m fields. The sizes of these local regions differ greatly (by a factor up to 10).

The graphene surface of the same chips was studied with a scanning electron microscope. The obtained images are shown in Fig. 5. Just as in AFM, the sizes of local regions differ by an order of magnitude. It is assumed that viruses and their aggregates of various sizes are visualized in local regions of AFM and SEM images. The inset in Fig 5, *b* (the overall inset size is 300×300 nm) shows that a small-sized (~ 100 nm) local region consists of finer particles. The correlation between SEM images of local graphene regions and viruses has been demonstrated in our earlier study [2]. Large (up to several micrometers) aggregates of influenza B virus imaged with a scanning electron microscope turned out to be identical to SEM images of pig influenza aggregates on other surfaces [21]. SEM images in

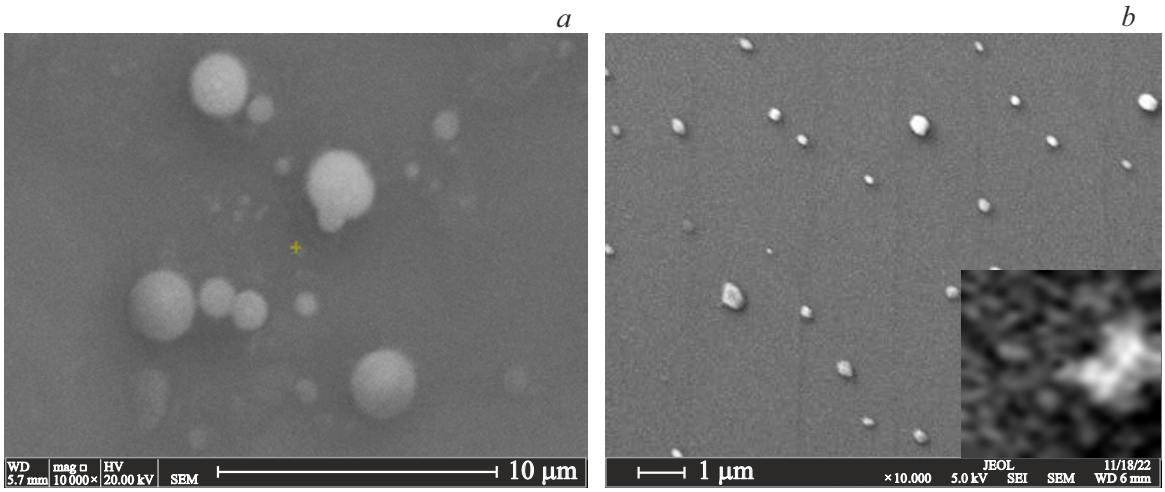

Figure 5. Images of the graphene surface in chips after detection of influenza B (a) and SARS-CoV-2 (b) viruses with similar concentrations of 10^{-9} g/mL. An enlarged image of a small local region (300×300 nm) is shown in the inset.

Fig. 5 reveal the presence of viruses of significantly varying sizes (this is especially true of SARS-CoV-2) on the surface. In the case of SARS-CoV-2, even local regions 100 nm in size turned out to be aggregates of finer particles (see the inset in Fig. 5, b). This immediately raises the issues of concentration dependence for the biosensor signal in the case of virus aggregation and of the influence of aggregates of various sizes on the shape of this dependence.

4. Conclusion

The results of examination of modification of adsorption properties of graphene in the process of topographic patterning of biosensor chips for influenza B and SARS-CoV-2 viruses by photolithography were reported. Graphene films were synthesized by thermal decomposition of SiC substrates. It was demonstrated experimentally that local regions emerging in the process of PLG as a result of interaction between benzene rings in graphene and the resist reduce the adsorption surface area of graphene. In addition, these regions enhance the non-uniformity of distributions of stresses and the free carrier density in graphene films. This modification of properties of graphene has a negative effect on the reproducibility of resistance of biosensor chips fabricated from the same wafer. It also reduces the efficiency of detection of viruses, potentially making the biosensor signal independent of the virus concentration. These negative effects may be minimized via AFM monitoring of the graphene surface state (in particular, quantitative monitoring by rms values) or by introducing a protective layer between graphene and resist layers in PLG. The best results in terms of virus detection were obtained in tests of chips with rms values after PLG differing by no more than 30% from the initial ones. These chips do not only manifest a concentration dependence, but also feature new local regions in AFM and SEM images of the graphene surface. The assumption of visualization of virus aggregates in the revealed local regions by these microscopy techniques and the significant size difference between aggregates of SARS-CoV-2 and influenza B viruses (the former are smaller than the latter) were discussed.

Conflict of interest

The authors declare that they have no conflict of interest.

References

[1] R.M. Torrente-Rodriguez, H. Lukas, J. Tu, J. Min, Y. Yang, C. Xu, H.B. Rossiter, W. Gao. Nature Biotechnol., **38**, 217 (2020).
[2] N.M. Shmidt, A.S. Usikov, E.I. Shabunina, A.V. Nashchekin, E.V. Gushchina, I.A. Eliseev, V.N. Petrov, M.V. Puzyk, O.V. Avdeev, S.A. Klotchenko, S.P. Lebedev, E.M. Tanklevskaya, Yu.N. Makarov, A.A. Lebedev, A.V. Vasin. Biosensors, **12**, 8 (2022).
[3] A.D. Da Silva, W.J. Paschoalino, J.P.V. Damasceno, L.T. Kubota. ChemElectroChem, **16**, 4508 (2020)
[4] D.M.A. Mackenzie, J.D. Buron, P.R. Whelan, J.M. Caridad, M. Bjergfelt, B. Luo, A. Shivayogimath, A.L. Smitshuysen, J.D. Thomsen, T.J. Booth, L. Gammelgaard, J. Zultak, B.S. Jessen, P. Bøggild, D.H. Petersen. Nano Research, **10**, 3596 (2017).
[5] I. Shtepliuk, F. Giannazzo, R. Yakimova. Appl. Sci., **11**, 5784 (2021).
[6] T.J.M. Fraga, M.N. Carvalho, M.G. Ghislandi, M.A. da Motta Sobrinho. Braz. J. Chem. Eng., **36**, 1 (2019).
[7] E.H. Lock, J.C. Prestigiacomo, P. Dev, A. Nath, R.L. Myers-Ward, T.L. Reinecke, D.K. Gaskill, M.S. Osofsky. Carbon, **175**, 490 (2021).
[8] G. Wu, X. Tang, M. Meyyappan, K.W.C. Lai. Appl. Surf. Sci., **425**, 713 (2017).

[9] M. M. Ali, J.J. Mitchell, G. Burwell, K. Rejnhard, C.A. Jenkins, E. Daghigh Ahmadi, S. Sharma, O.J. Guy. Nanomaterials, **11**, 2121 (2021).
[10] K. Kumar, Y.S. Kim, E.H. Yang. Carbon, **65**, 35 (2013).
[11] Sh.-W. Lee, M. Muoth, T. Helbling, M. Mattmann, Ch. Hierold. Carbon, **66**, 295 (2014).
[12] A. Choi, A. Tuan Hoang, T.Th. Ngoc Van, B. Shong, L. Hu, K.Y. Thai, J.-H. Ahn. Chem. Eng. J., **429**, 132504 (2022).
[13] Ch-Y. Zhu, S. Peng, X. Zhang, Y. Yao, X. Huang, Y. Yan, D. Zhang, J. Shi, Zh. Jin. Nanotechnology, **32**, 315201 (2021).
[14] A.A. Lebedev, V.Y. Davydov, D.Y. Usachov. J. Phys. Conf. Ser., **951**, 012007 (2018).
[15] A. Usikov, K. Borodkin, S. Novikov, A. Roenkov, A. Goryachkin, M. Puzyk, I. Barash, S. Lebedev, S.A. Zubov, Y. Makarov. Proc. Est. Acad. Sci., **68**, 207 (2019).
[16] V.Yu. Davydov, D.Yu. Usachov, S.P. Lebedev, A.N. Smirnov, V.S. Levitskii, I.A. Eliseyev, P.A. Alekseev, M.S. Dunaevskiy, O.Yu. Vilkov, A.G. Rybkin, A.A. Lebedev. Semiconductors, **51** (8), 1072 (2017).
[17] T. Wang, J.R. Huntzinger, M. Bayle, C. Roblin, J.M. Decams, A.A. Zahab, S. Contreras, M. Paillet, P. Landois. Carbon, **163**, 224 (2020).
[18] J.E. Lee, G. Ahn, J. Shim, Y.S. Lee, S. Ryu. Nature Commun., **3** (1), 1024 (2012).
[19] I.A. Eliseyev, V.Yu. Davydov, A.N. Smirnov, M.O. Nestoklon, P.A. Dementev, S.P. Lebedev, A.A. Lebedev, A.V. Zubov, S. Mathew, J. Pezoldt, K.A. Bokai, D.Yu. Usachov. Semiconductors, **53** (14), 1904 (2019).
[20] Zh. Gao, H. Kang, C.H. Naylor, F. Streller, P. Ducos, M.D. Serrano, J. Ping, J. Zauberman, R.W. Carpick, Y.-J. Wang, Y.W. Park, Zh. Luo, L. Ren, A.T.Ch. Johnson. ACS Appl. Mater. Interfaces, **8**, 27546 (2016).
[21] Science Photo Library. Available online: sciencephoto.com/media/249227/view/coloured-sem-of-influenza-virus-on-cell-surface (accessed on 09.12.2022).